

Supporting Information

Accelerating solid diffusion and suppressing phase transition in LiV_3O_8 via calcium doping at lithium sites

Yinsheng Xu^a, Xiaoxiao Wang^a, Zhengnan Wang^a, Shengping Wang^{a, *}, Xiaoyan Zhu^{a, *}, Daoyu
Li^b, Jingxian Yu^{c, *}

^a Faculty of Materials Science and Chemistry, China University of Geosciences, Wuhan 430074,
China

^b Guiyang Bureau, Extra High Voltage Power Transmission Company, China Southern Power Grid
(CSG), Guiyang 550081, China

^c ARC Centre of Excellence for Nanoscale BioPhotonics (CNBP), School of Chemistry and Physics,
The University of Adelaide, Adelaide, SA 5005, Australia

* Corresponding Author. spwang@cug.edu.cn (S. Wang), bright_xyz@126.com (X. Zhu), Jingxian.Yu@adelaide.edu.au (J. Yu)

Table S1 Lattice parameters of the samples.

Samples	Interlayer distance (Å)	a (Å)	b (Å)	c (Å)	β (°)	V (Å ³)
Ca-0.00	6.317	6.630	3.599	12.026	107.795	286.684
Ca-0.01	6.328	6.646	3.595	12.032	107.802	287.190
Ca-0.03	6.329	6.649	3.600	12.033	107.858	287.775
Ca-0.05	6.340	6.660	3.596	12.038	107.854	288.028
Ca-0.07	6.346	6.670	3.598	12.039	107.850	288.652
Ca-0.10	6.341	6.662	3.596	12.027	107.865	287.824

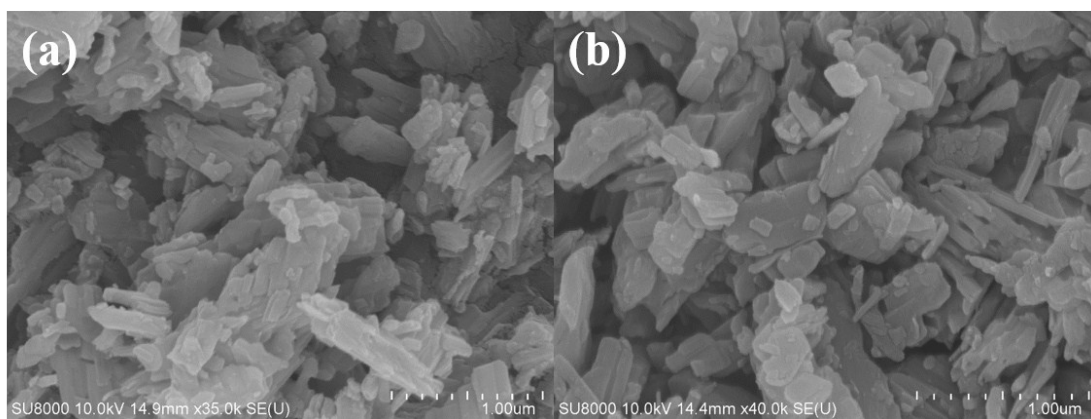


Figure S1 SEM images of Ca-0.00 (a) and Ca-0.07 (b).

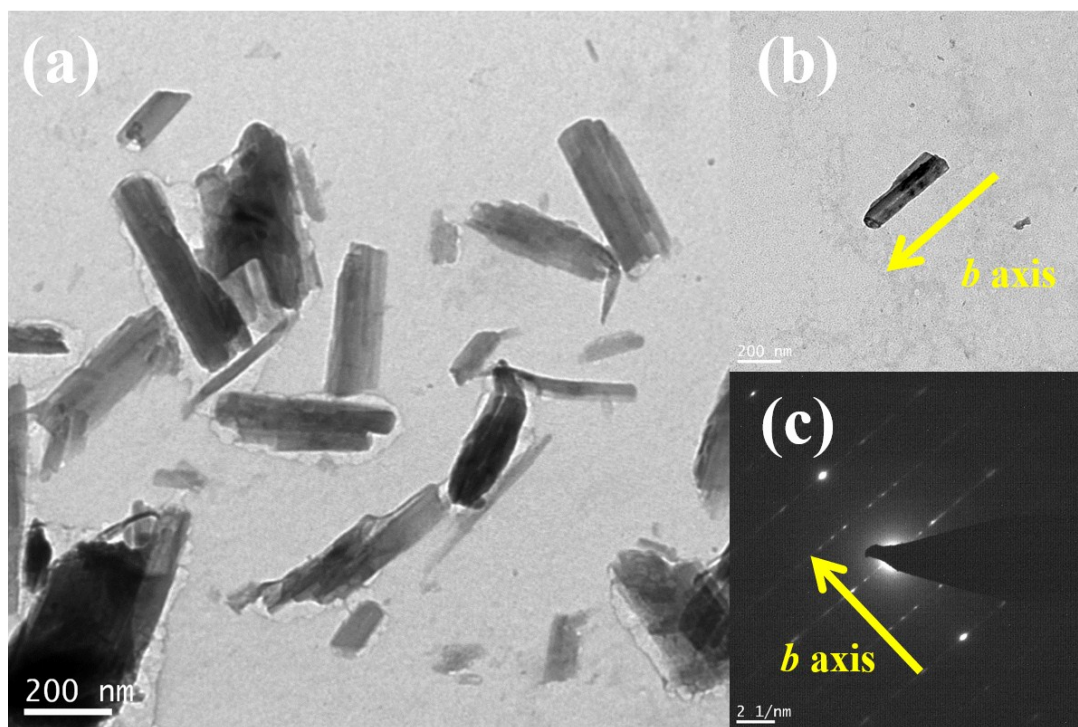


Figure S2 TEM images (a, b) and SAED pattern (c) of Ca-0.00 in (b) along the [100] zone axis.

Table S2 Cell parameters from experiments and calculations of the undoped and Ca-doped LiV_3O_8 .

	Experimental data			Computational data	
	Ca-0.00	Ca-0.07	undoped	Ca-substituted Li	Ca-substituted V
a (Å)	6.630	6.670	6.453	6.470	6.392
b (Å)	3.599	3.595	3.566	3.568	3.600
c (Å)	12.026	12.039	11.816	11.835	11.854
β (°)	107.795	107.850	107.791	107.866	105.962

In this work, first-principles calculation was employed to determine the real sites of calcium doping. For the crystal structures of Ca-doped LiV_3O_8 , a $3 \times 3 \times 1$ supercell was used and the central two lithium atoms were replaced with one calcium. This supercell possessed a Ca/Li atomic ratio of 6.25%, close to the experimental ratio of 7%. The cell parameters of pure, Ca-substituted-V and Ca-substituted-Li LiV_3O_8 were compared. As shown in Table S2, the lattice parameters obtained from experiments and calculations are quite consistent for pure and Ca-substituted-V LiV_3O_8 . The lattice parameter a related to the interlayer distance is considered an important parameter of crystal structure for LiV_3O_8 . The lattice parameters a of pure and Ca-substituted-Li LiV_3O_8 were 6.453 and 6.470 Å, respectively. Substituting Ca for V, resulted in reduction of lattice parameters a , which was contrary to the experimental results. Therefore, the conclusion that lithium, not vanadium, were replaced by calcium, can be obtained through a combination method of the calculation and experiment.

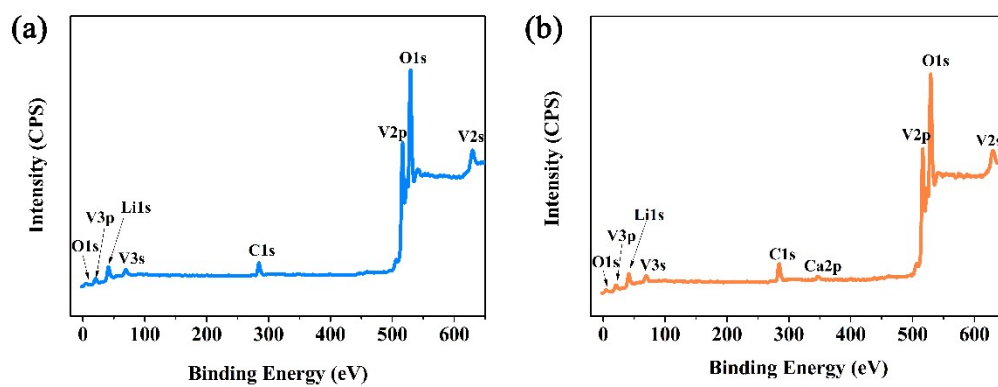


Figure S3 XPS survey spectra of Ca-0.00 (a) and Ca-0.07 (b).

Table S3 Electrochemical performance comparison of the hewettite group.

Typical example	Material synthesis	Electrochemical performance	Reference
$\text{Li}_{1.1}\text{V}_3\text{O}_8$	sol-gel	206 mAh g^{-1} after 100 cycles at 30 mA g^{-1}	[1]
$\text{Li}_{1.5}\text{V}_3\text{O}_8$	sol-gel	100 mAh g^{-1} after 100 cycles at 175 mA g^{-1}	[2]
$\text{LiV}_3\text{O}_8/\text{PDPA}$	Composite	125 mAh g^{-1} after 50 cycles at 2000 mA g^{-1}	[3]
LiV_3O_8	hydrothermal	150 mAh g^{-1} after 100 cycles at 1000 mA g^{-1}	[4]
LiV_3O_8	Ni doping	251 mAh g^{-1} after 30 cycles at 150 mA g^{-1}	[5]
LiV_3O_8	Ga doping	226 mAh g^{-1} after 50 cycles at 30 mA g^{-1}	[6]
LiV_3O_8	Mo doping	206 mAh g^{-1} after 100 cycles at 300 mA g^{-1}	[7]
LiV_3O_8	Na doping	230 mAh g^{-1} after 50 cycles at 150 mA g^{-1}	[8]
NaV_3O_8	hydrothermal	167 mAh g^{-1} after 100 cycles at 150 mA g^{-1}	[9]
$\text{Na}_{1.08}\text{V}_3\text{O}_8$	hydrothermal	170 mAh g^{-1} after 200 cycles 600 mA g^{-1}	[10]
$\text{Na}_2\text{V}_6\text{O}_{16}$	hydrothermal	170 mAh g^{-1} after 100 cycles 300 mA g^{-1}	[11]
LiV_3O_8	Ca doping	170 mAh g^{-1} after 400 cycles 1000 mA g^{-1} 256 mAh g^{-1} after 100 cycles 150 mA g^{-1}	Our work

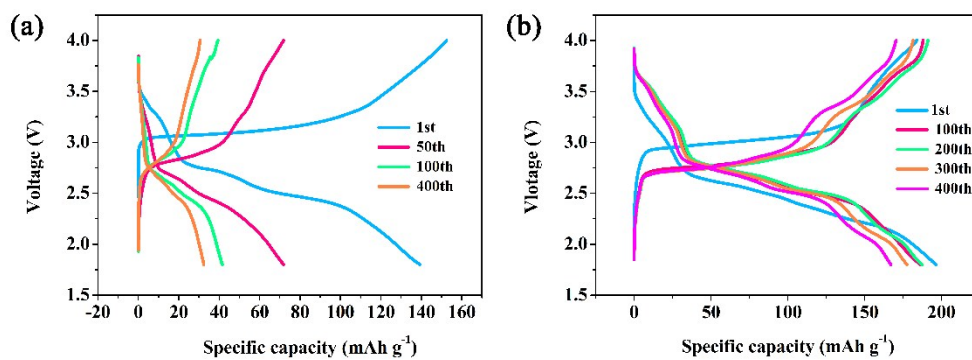


Figure S4 Charge-discharge curves of Ca-0.00 (a) and Ca-0.07 (b) at 1000 mA g⁻¹.

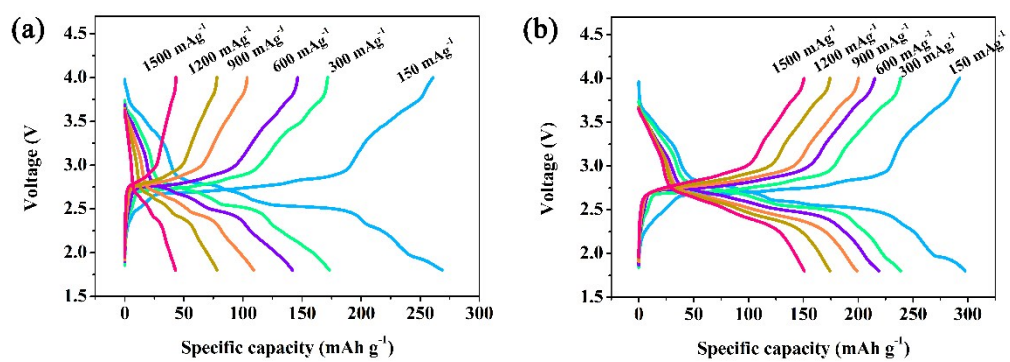


Figure S5 Charge-discharge curves of Ca-0.00 (a) and Ca-0.07 (b).

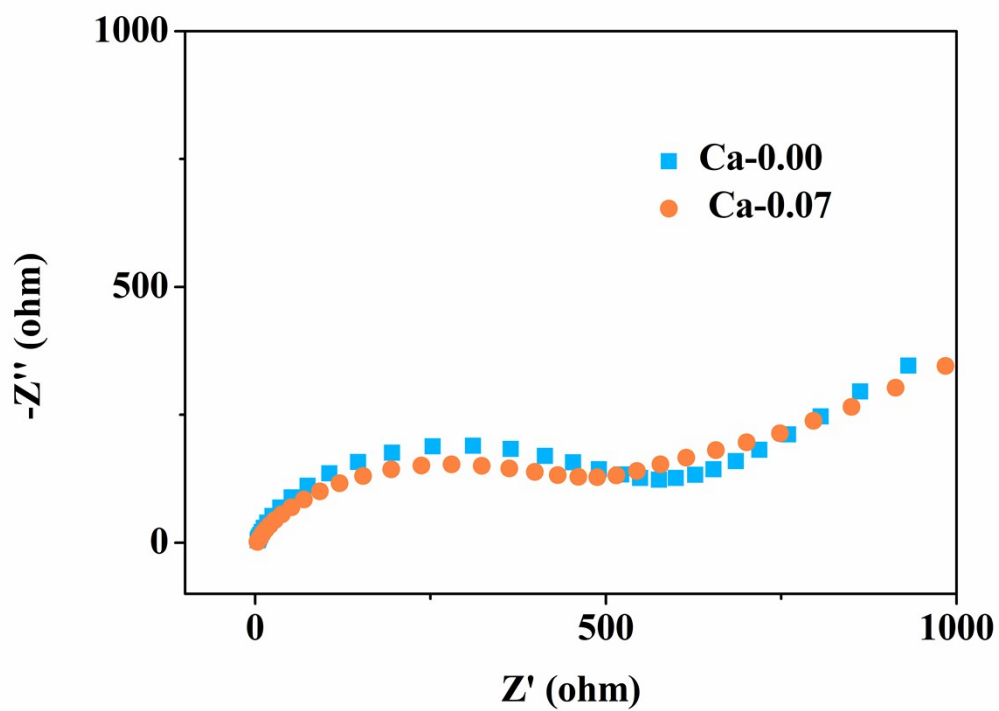


Figure S6 Nyquist plots of Ca-0.00 and Ca-0.07 before cycling. Both Ca-0.00 and Ca-0.07 without charge and discharge processes had a large impedance for the unactivated electrode.

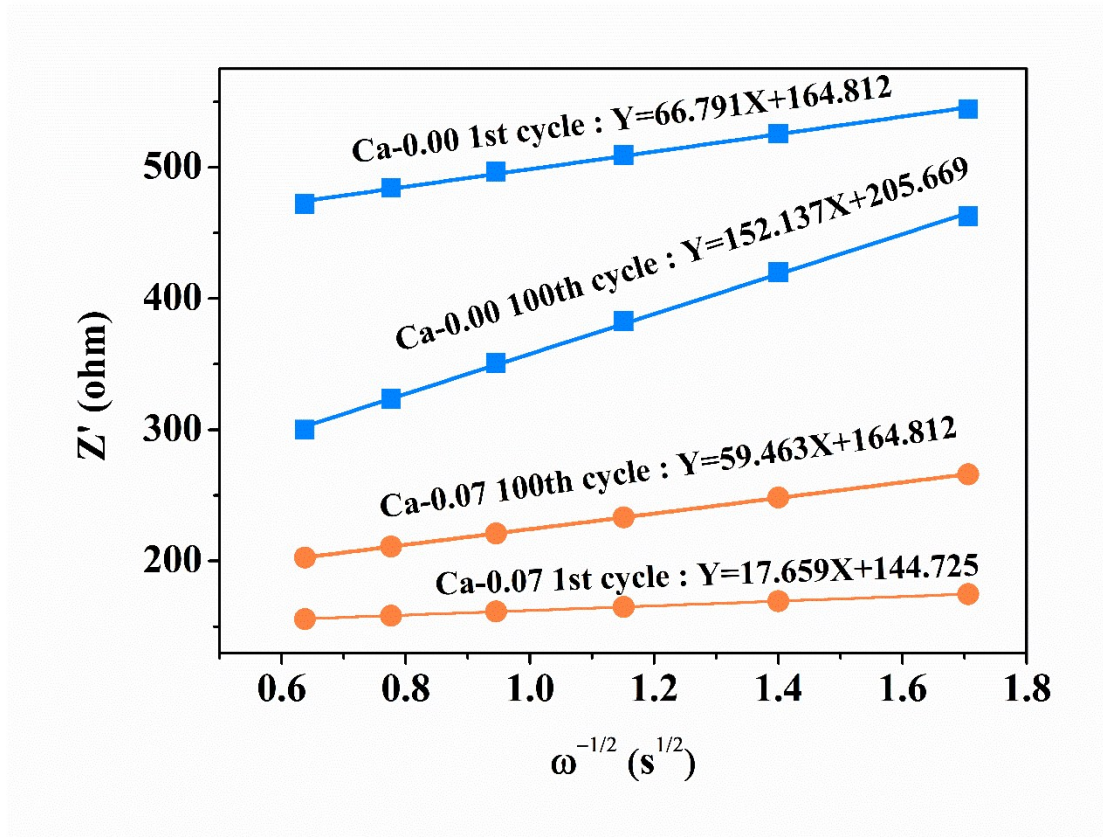


Figure S7 Relationship curves between Z' and $\omega^{-1/2}$ in the low frequency range.

The Li⁺ diffusion coefficient by EIS

The Nyquist plots exhibited a semicircle in the high frequency range and a sloped line in the low frequency range. The semicircle represents the charge transfer process (R_{ct}) at the solid-liquid interface, and the sloped line represents the Warburg impedance (Z_W) at a low frequency, which results from Li⁺ diffusion in the LiV₃O₈ matrix. The Li⁺ diffusion coefficient could be calculated from the low frequency plots based on [Formulas S1 and S2](#):

$$Z' = R_s + R_{ct} + \sigma_W \omega^{-1/2} \quad (S1)$$

$$D_{Li^+} = \frac{R^2 T^2}{2A^2 n^2 F^4 C^2 \sigma_W^2} \quad (S2)$$

where ω ($2\pi f$) is the angular frequency in the low frequency region, R is the gas constant, T is the temperature, A is the area of the electrode, n is the number of electrons transferred per mole of active material involved in the electrode reaction, F is the Faraday constant, and C is the molar concentration of lithium ions.

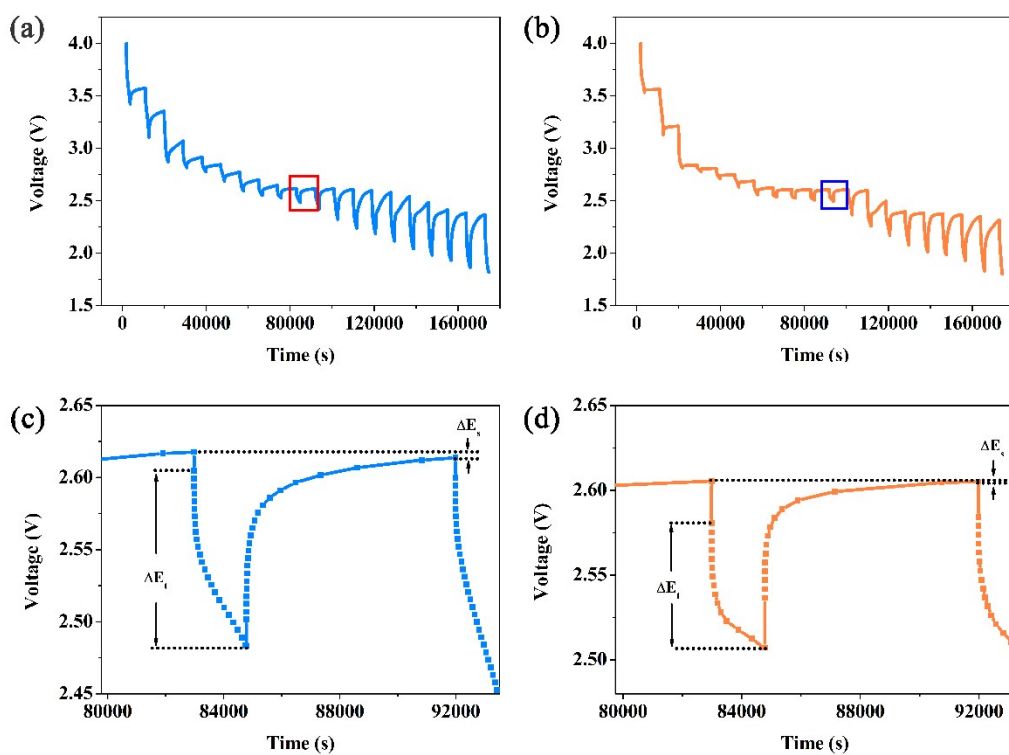


Figure S8 GITT curves and magnified views of Ca-0.00 (a, c) and Ca-0.07 (b, d).

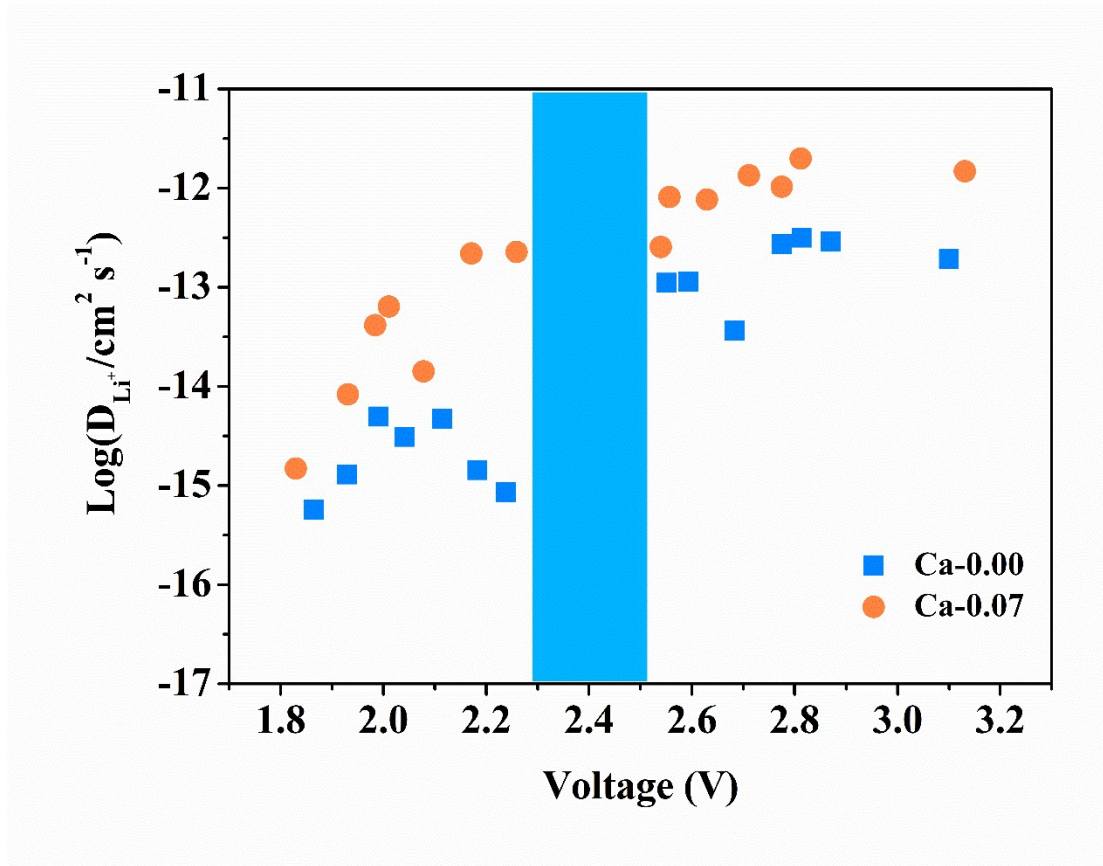


Figure S9 Li⁺ diffusion coefficients of Ca-0.00 and Ca-0.07.

The Li⁺ diffusion coefficient by GITT

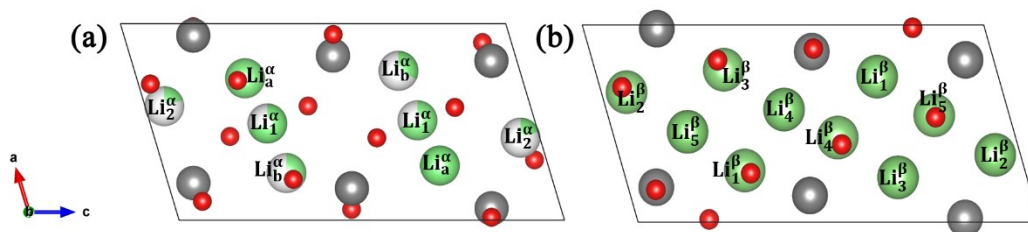
Although the Li⁺ diffusion coefficient could not be reliably obtained by GITT in the two-phase region, as previously discussed, it could be determined accurately in the solid solution region. The Li⁺ diffusion coefficients are shown in Figure S9 and are calculated based on Formula S3 [12]:

$$D_{\text{Li}^+} = \frac{4}{\pi\tau} \left(\frac{n_m V_m}{S} \right)^2 \left(\frac{\Delta E_s}{\Delta E_t} \right)^2 \quad (\text{S3})$$

where τ is the pulse time, n_m is the molar number, V_m is the molar volume of the electrode, S is the geometric area of the sample-electrolyte interface, ΔE_s is the change in the steady-state voltage of the cell for this step, and ΔE_t is the total transient voltage change of the cell for the applied current at time τ .

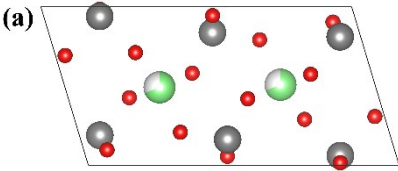
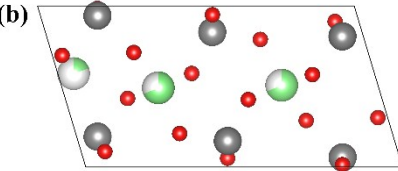
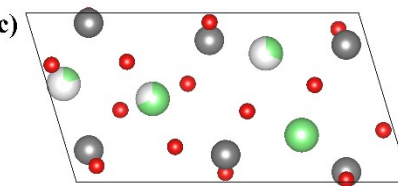
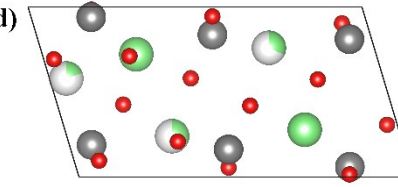
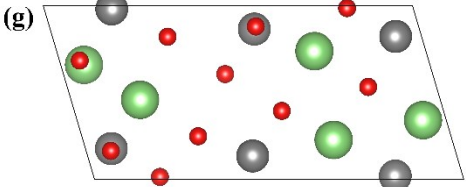
All the available Li sites and corresponding labeling for both phases

All the available Li sites and corresponding labeling for both the alpha and beta phases are shown in [Figure S10](#), which is referred to in [Reference \[13\]](#).

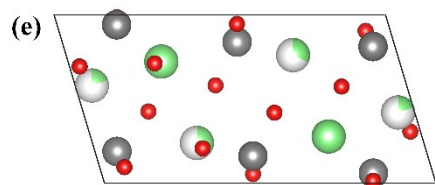


[Figure S10](#) Lithium sites and labeling for both the alpha (a) and beta (b) phases. The green balls are lithium atoms, the gray balls are vanadium atoms, and the red balls are oxygen atoms.

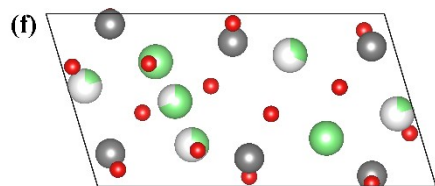
Table S4 Lithium configurations for the lowest energy states of bare LiV_3O_8 in the alpha (a-f) phase and beta (g-l) phase.

	alpha phase	beta phase
$\text{Li}_1\text{V}_3\text{O}_8$	(a) 	
$\text{Li}_{1.5}\text{V}_3\text{O}_8$	(b) 	
$\text{Li}_2\text{V}_3\text{O}_8$	(c) 	
$\text{Li}_{2.5}\text{V}_3\text{O}_8$	(d) 	(g) 

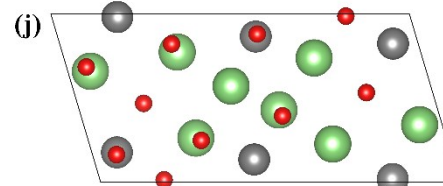
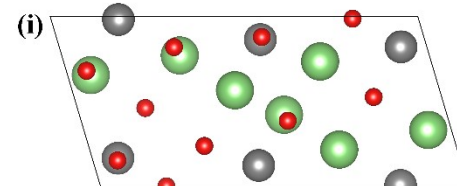
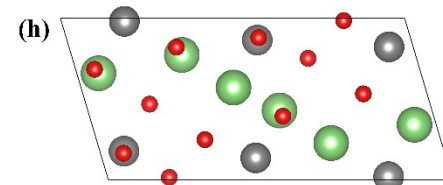
$\text{Li}_3\text{V}_3\text{O}_8$



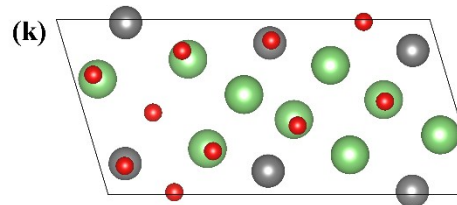
$\text{Li}_{3.5}\text{V}_3\text{O}_8$

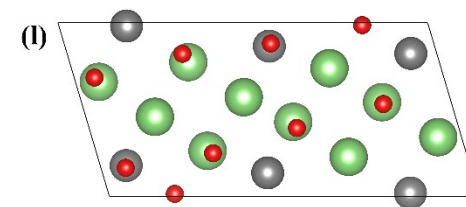
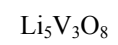


$\text{Li}_4\text{V}_3\text{O}_8$



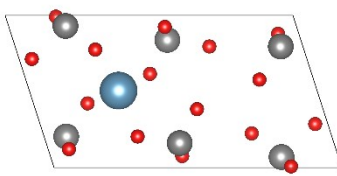
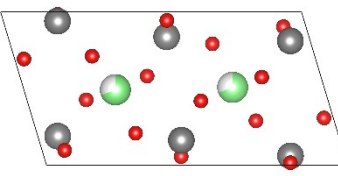
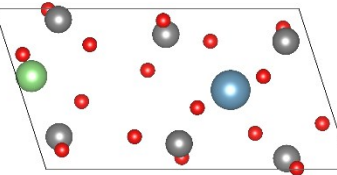
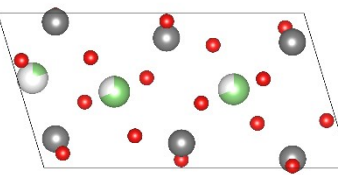
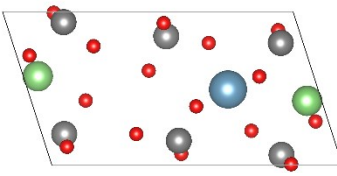
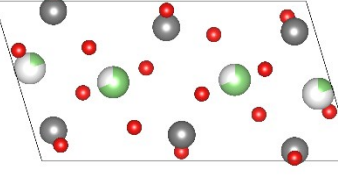
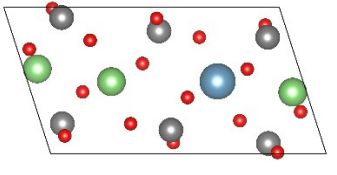
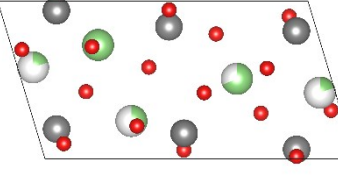
$\text{Li}_{4.5}\text{V}_3\text{O}_8$

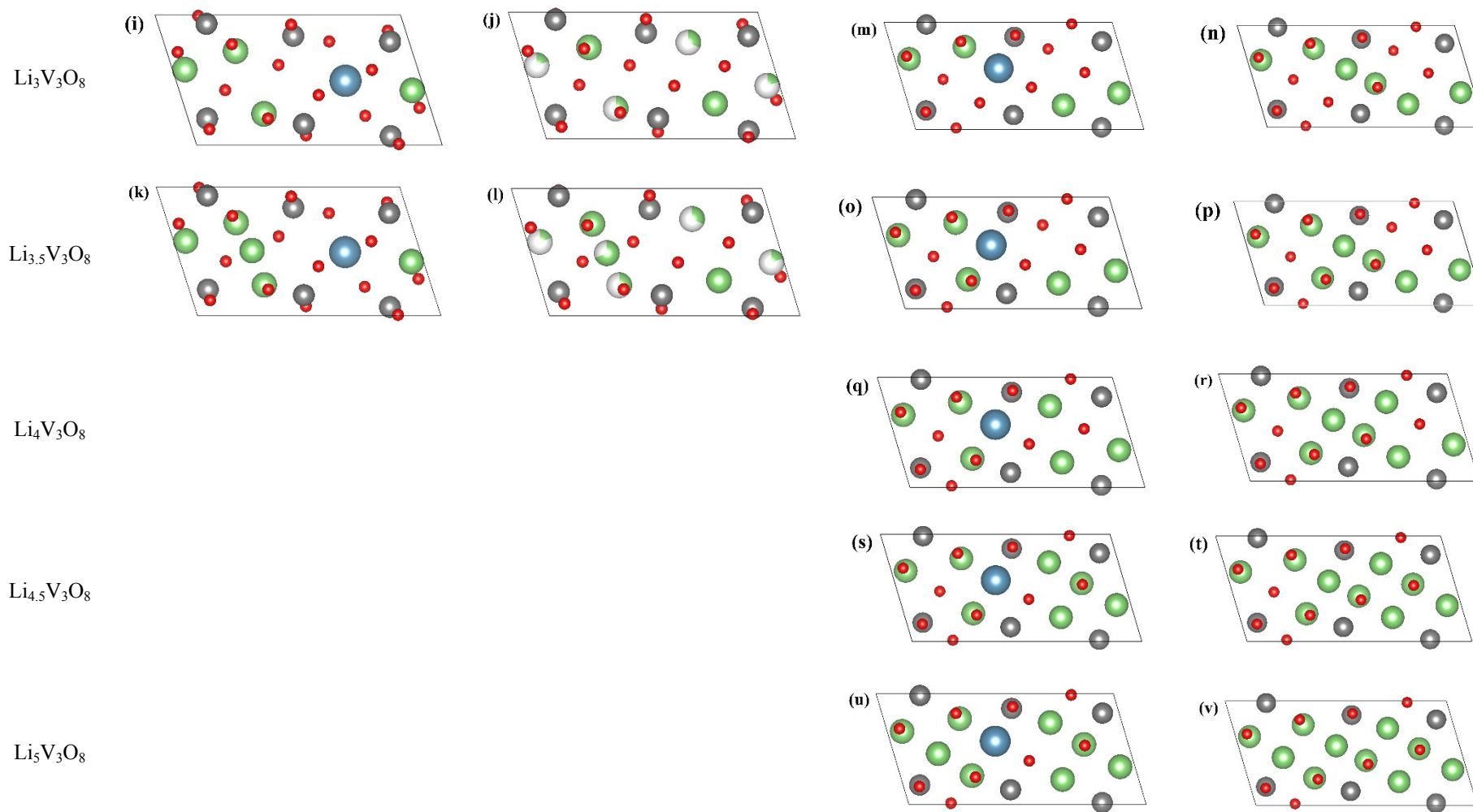




The figures in [Table S4](#) correspond to [Figure S11](#) in this paper.

Table S5 Lithium configurations for the lowest energy states of Ca-doped LiV_3O_8 in the alpha phase (a-l) and beta phase (m-v).

		alpha phase		beta phase		
		Ca-containing cell	Ca-free cell	Ca-containing cell	Ca-free cell	
$\text{Li}_1\text{V}_3\text{O}_8$	(a)		(b)			
$\text{Li}_{1.5}\text{V}_3\text{O}_8$	(c)		(d)			
$\text{Li}_2\text{V}_3\text{O}_8$	(e)		(f)			
$\text{Li}_{2.5}\text{V}_3\text{O}_8$	(g)		(h)			



The figures in [Table S5](#) correspond to [Figure S12](#) in this paper.

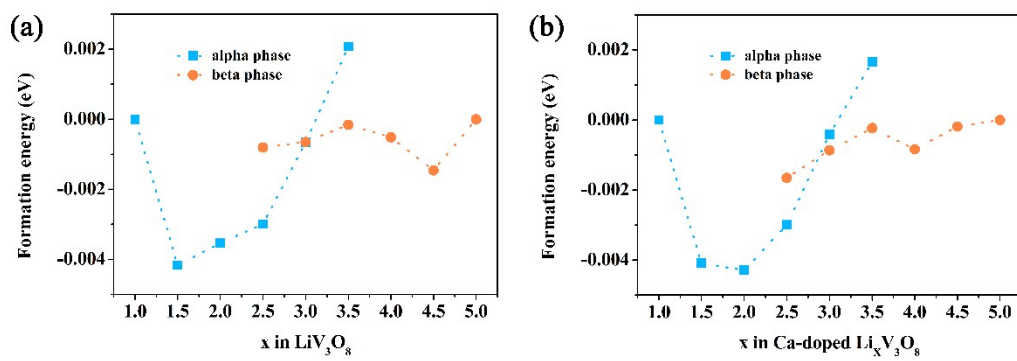


Figure S13 Formation energies for the lowest energy states of LiV_3O_8 (a) and Ca-doped LiV_3O_8 (b).

References

- [1] Q. Zhang, A.B. Brady, C.J. Pelliccione, D.C. Bock, A.M. Bruck, J. Li, V. Sarbada, R. Hull, E.A. Stach, K.J. Takeuchi, E.S. Takeuchi, P. Liu, A.C. Marschilok, Investigation of structural evolution of $\text{Li}_{1.1}\text{V}_3\text{O}_8$ by in situ X-ray diffraction and density functional theory calculations, *Chem. Mater.*, 2017, 29, 2364-2373. <https://doi.org/10.1021/acs.chemmater.7b00096>
- [2] Y. Wang, X. Xu, C. Cao, C. Shi, W. Mo, H. Zhu, Synthesis and performance of $\text{Li}_{1.5}\text{V}_3\text{O}_8$ nanosheets as a cathode material for high-rate lithium-ion batteries, *J. Power Sources*, 2013, 242, 230-235. <https://doi.org/10.1016/j.jpowsour.2013.05.059>
- [3] L. Zhu, L. Xie, X. Cao, LiV_3O_8 /polydiphenylamine composites with significantly improved electrochemical behavior as cathode materials for rechargeable lithium batteries, *ACS Appl. Mater. Interfaces*, 2018, 10, 10909-10917. <https://doi.org/10.1021/acsami.8b00364>
- [4] H. Wang, Y. Ren, Y. Wang, W. Wang, S. Liu, Synthesis of LiV_3O_8 nanosheets as a high-rate cathode material for rechargeable lithium batteries, *CrystEngComm*, 2012, 14, 2831. <https://doi.org/10.1039/c2ce06326c>
- [5] L. Liu, L. Jiao, J. Sun, Y. Zhang, M. Zhao, H. Yuan, Y. Wang, Electrochemical performance of $\text{LiV}_{3-x}\text{Ni}_x\text{O}_8$ cathode materials synthesized by a novel low-temperature solid-state method, *Electrochim. Acta*, 2008, 53, 7321-7325. <https://doi.org/10.1016/j.electacta.2008.03.056>
- [6] X. Ren, S. Hu, C. Shi, P. Zhang, Q. Yuan, J. Liu, Preparation of Ga-doped lithium trivanadates as cathode materials for lithium-ion batteries, *Electrochim. Acta*, 2012, 63, 232-237. <https://doi.org/10.1016/j.electacta.2011.12.099>
- [7] H. Song, Y. Liu, C. Zhang, C. Liu, G. Cao, Mo-doped LiV_3O_8 nanorod-assembled nanosheets as a high performance cathode material for lithium ion batteries, *J. Mater. Chem. A*, 2015, 3, 3547-3558. <https://doi.org/10.1039/C4TA05616G>
- [8] X. Lu, S. Yu, S. Zhang, D. Chao, Enhanced lithium ion transport by superionic pathways formed on the surface of two-dimensional structured $\text{Li}_{0.85}\text{Na}_{0.15}\text{V}_3\text{O}_8$ for high-performance lithium ion batteries, *Electrochim. Acta*, 2015, 155, 148-156. <https://doi.org/10.1016/j.electacta.2014.12.119>
- [9] Y. Tang, D. Sun, H. Wang, X. Huang, H. Zhang, S. Liu, Y. Liu, Synthesis and electrochemical properties of NaV_3O_8 nanoflakes as high-performance cathode for Li-ion battery, *RSC Adv.*, 2014, 4, 8328-8334. <https://doi.org/10.1039/C3RA44733B>
- [10] H. Wang, S. Liu, Y. Ren, W. Wang, A. Tang, Ultrathin $\text{Na}_{1.08}\text{V}_3\text{O}_8$ nanosheets-a novel cathode material with superior rate capability and cycling stability for Li-ion batteries, *Energy Environ. Sci.*, 2012, 5, 6173-6179. <https://doi.org/10.1039/C2EE03215E>
- [11] H. Wang, W. Wang, Y. Ren, K. Huang, S. Liu, A new cathode material $\text{Na}_2\text{V}_6\text{O}_{16} \cdot x\text{H}_2\text{O}$ nanowire for lithium ion battery, *J. Power Sources*, 2012, 199, 263-269. <https://doi.org/10.1016/j.jpowsour.2011.10.045>
- [12] W. Weppner, R.A. Huggins, Determination of the kinetic parameters of mixed-conducting electrodes and application to the system Li_3Sb , *J. Electrochem. Soc.*, 1977, 124, 1569-1578.

<https://doi.org/10.1149/1.2133112>

- [13] T. Jiang, M.L. Falk, Calculations of the thermodynamic and kinetic properties of $\text{Li}_{1+x}\text{V}_3\text{O}_8$, *Phys. Rev. B*, 2012, 85, 245111. <https://doi.org/10.1103/PhysRevB.85.245111>